



Nickel–lithium oxide alloy transparent conducting films deposited by spray pyrolysis technique

Hasan Azimi Juybari^a, Mohammad-Mehdi Bagheri-Mohagheghi^a, Mehrdad Shokooh-Saremi^{b,*}

^a School of Physics, Damghan University, Damghan, Iran

^b Department of Electrical Engineering, Ferdowsi University of Mashhad, Mashhad, Iran

ARTICLE INFO

Article history:

Received 26 June 2010

Received in revised form 2 November 2010

Accepted 14 November 2010

Available online 21 November 2010

Keywords:

Transparent conducting oxides

Spray pyrolysis

Nickel oxide

Lithium doping

ABSTRACT

In this research, nickel oxide (NiO) transparent semiconducting films are prepared by spray pyrolysis technique on glass substrates. The effect of Ni concentration in initial solution and substrate temperature on the structural, electrical, thermoelectrical, optical and photoconductivity properties of NiO thin films are studied. The results of investigations show that optimum Ni concentration and suitable substrate temperature for preparation of basic undoped NiO thin films with p-type conductivity and high optical transparency is 0.1 M and 450 °C, respectively. Then, by using these optimized deposition parameters, nickel–lithium oxide ((Li:Ni)O_x) alloy films are prepared. The XRD structural analysis indicate the formation of the cubic structure of NiO and (Li:Ni)O_x alloy films. Also, in high Li doping levels, Ni₂O₃ and NiCl₂ phases are observed. The electrical measurements show that the resistance of the films decreases with increasing Li level up to 50 at%. For these films, the optical band gap and carrier concentration are obtained to be 3.6 eV and 10¹⁵–10¹⁸ cm⁻³, respectively.

© 2010 Elsevier B.V. All rights reserved.

1. Introduction

Transparent conducting oxides (TCOs) have been extensively studied in recent years since they not only exhibit high optical transparency in the visible region but also the high electrical conductivity [1–3]. TCOs, such as ITO, ZnO and SnO₂ are widely used in a variety of optoelectronic devices [4–6].

In contrast to n-type TCOs (like SnO₂, In₂O₃, and ZnO), nickel oxide (NiO) shows p-type semiconductivity and has attracted much attention due to its excellent chemical stability and unique optical, electrical and magnetic properties. Nickel oxide has found important applications in electro-chromic devices, organic light emitting diodes, chemical sensors, dye sensitized solar cells, and thin film p–n junctions [7–11]. Undoped NiO has a wide direct band gap of 3.5–4 eV [12,13] and exhibits low p-type conductivity. Its resistivity can be decreased by doping with monovalent impurities, such as lithium (Li) [14–16]. In 2003, Ohta et al. fabricated an ultraviolet detector based on lithium-doped NiO (NiO:Li) and ZnO films [17]. Recently, NiO thin films with switching properties suitable for memory devices have been fabricated by reactive sputtering [18].

NiO films have been prepared by variety of physical and chemical techniques, such as sputtering, pulsed laser deposition (PLD), chemical vapor deposition (CVD), electron beam evaporation,

sol–gel, and spray pyrolysis technique [19–25]. The spray pyrolysis (SP) technique is a very important method for preparation of transparent conducting oxide films. Spray pyrolysis is a relatively simple, atmospheric pressure deposition method and an inexpensive technique for large-area coating. However, few efforts have been made to systematically investigate the effect of deposition parameters and Li impurity on the electrical and thermo-electrical properties of the NiO thin films fabricated by spray pyrolysis technique.

In this research, we investigate the effect of the deposition parameters, such as substrate temperature and Li concentration level (in precursor solution), on the physical properties of the NiO films prepared by spray pyrolysis method. The electrical, thermo-electrical, structural and optical properties of these films are studied using Hall effect and Seebeck measurements, X-ray diffraction (XRD), Scanning electron microscopy (SEM) analysis and UV–vis absorption spectroscopy.

2. Experimental procedure

Undoped NiO and (Li:Ni)O_x alloy thin films were deposited on glass substrate by spray pyrolysis technique. For deposition of undoped films, certain amount of nickel nitrate hexa-hydrate (Ni(NO₃)₂·6H₂O) was dissolved in distilled water to make initial (precursor) solution. For alloy films, the precursor solution was prepared by dissolving Ni(NO₃)₂·6H₂O and different amounts of lithium chloride (LiCl) in distilled water. The [Li]/[Ni] atomic ratio was 0–100 at%. The NiO and (Li:Ni)O_x films were deposited under the similar conditions: solution volume (V) = 30 ml, deposition rate (R) = 10 ml/min, nozzle to substrate distance (d) = 35 cm. Compressed air was used as the carrier gas. We optimized the Ni concentration and the substrate temperature for deposition of the basic undoped NiO films, which will be presented in Section 3.

* Corresponding author.

E-mail address: mehrdad.s.saremi@gmail.com (M. Shokooh-Saremi).

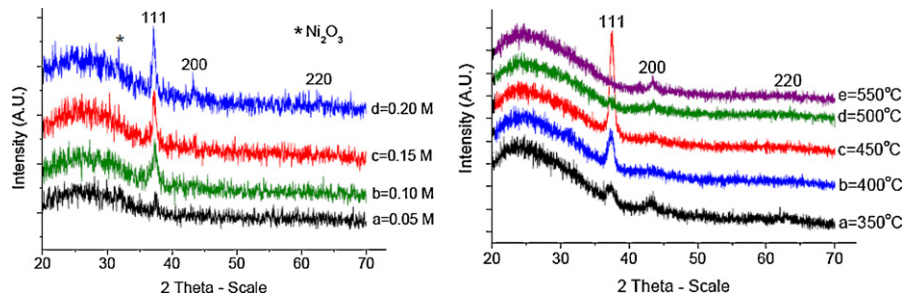


Fig. 1. (a) The XRD patterns of NiO films prepared with different Ni concentration in precursor solution and $T_{\text{sub}} = 450^\circ\text{C}$. (b) The XRD patterns of NiO films deposited at various substrate temperatures for 0.1 M Ni concentration.

The sheet resistance (R_s) of the films was measured by two-point probe method using thermally evaporated aluminum electrodes. The concentration and type of the majority carriers was determined by Hall effect experiment. Majority carrier concentration was determined using the following equation [26]:

$$N_{n,p} = \frac{IB}{|q|V_H t} \quad (1)$$

where I , B , t , q and V_H are the measured current, magnetic flux density, film thickness, electron charge and Hall voltage, respectively. By applying a temperature gradient between the two ends of the samples, the thermoelectric e.m.f. of the prepared films was measured and then the Seebeck coefficients were determined by calculating the slope of the thermoelectric e.m.f. versus temperature difference.

For structural study of the films, XRD patterns of the NiO and (Li:Ni) O_x films were recorded by D8 Advance Bruker system using Cu $K\alpha$ ($\lambda = 0.15406$ nm) radiation. The average crystallite size (D) was calculated using the Scherrer's formula [26]:

$$D = \frac{k\lambda}{\delta w \cos \theta} \quad (2)$$

where δw is the full width at half maximum (FWHM) of the corresponding XRD peak, k is a constant (~ 1) and θ is the Bragg angle.

Surface morphology of the films was observed by Philips XL-30 SEM system. The optical measurements were carried out in the range of 190–1100 nm using Unico 4802 spectrophotometer system. The direct band gap (E_g) of the prepared films was obtained from the extrapolation of the linear part of the $(\alpha h\nu)^2$ curve versus photon energy ($h\nu$) and using the following equation [27]:

$$(\alpha h\nu)^2 = A(h\nu - E_g) \quad (3)$$

where α and E_g are the absorption coefficient and the energy gap, respectively, and A is a constant.

3. Results and discussion

3.1. Structural and electrical properties

To find the optimal parameters for deposition of the basic undoped NiO films (Ni concentration in solution and substrate temperature), two sets of experiments were carried out. To obtain the appropriate concentration, Ni molarities in solution was changed from 0.05 to 0.2 M and substrate temperature kept at 450°C . Then, in order to study the effect of substrate temperature, NiO thin films were prepared in different temperatures (350 – 550°C) in optimum concentration found from the first set of experiments. After that (Li:Ni) O_x films were deposited on glass substrate with precursors with optimal Ni concentration and optimal substrate temperature.

Fig. 1(a) shows the XRD patterns of the NiO films prepared with different nickel concentrations. As seen, all films have polycrystalline NiO phase with a cubic structure and preferred orientation along (1 1 1) direction. The intensity of the peaks corresponding to the (1 1 1), (2 0 0) and (2 2 0) orientations increases with Ni molarity increase in the solution. In addition, this increase in the intensity of the peaks may be attributed either to the grain growth associated with larger thicknesses, or the increase in the degree of crystallinity by increasing the solution molarity [28]. Also, in the XRD patterns corresponding to the higher Ni concentrations (0.15 M and 0.2 M),

Ni_2O_3 phase is observed. Based on this figure, films prepared with 0.1 M of Ni in solution show the best single phase characteristics.

The X-ray diffraction patterns of NiO films deposited at different substrate temperatures are shown in Fig. 1(b), keeping Ni concentration at 0.1 M. The films show cubic NiO crystallographic lattice with preferred orientation along (1 1 1) direction. The intensity of the (1 1 1) peak increases with increasing the substrate temperature from 350°C to 450°C and then decreases [29]. For preparation of the alloy films, we kept Ni concentration and substrate temperature at 0.1 M and 450°C (as the optimal deposition parameters), respectively.

Fig. 2 shows the XRD patterns of the deposited (Li:Ni) O_x alloy films with different Li doping levels from 0 at% to 100 at% in the solution. As seen, all films are polycrystalline and all the crystallographic peaks belong to the cubic NiO phase with preferred orientation along (1 1 1) direction. At 50 at% Li doping level, the intensity of the peak corresponding to the (1 1 1) plane is the strongest, however, at higher doping levels, other phases such as Ni_2O_3 and NiCl_2 are observed.

The XRD parameters and mean grain size of the undoped NiO and (Li:Ni) O_x alloy films for (1 1 1) crystallographic orientation, have been summarized in Table 1.

Scanning electron microscopy (SEM) micrographs of the (Li:Ni) O_x alloy films are shown in Fig. 3(a)–(f). The micrographs show that the nanostructure of the films exhibits the particle-cluster type growth. The undoped NiO film has a nearly smooth surface; however the (Li:Ni) O_x films have a porous structure and their corresponding grain size increases with increasing the doping level.

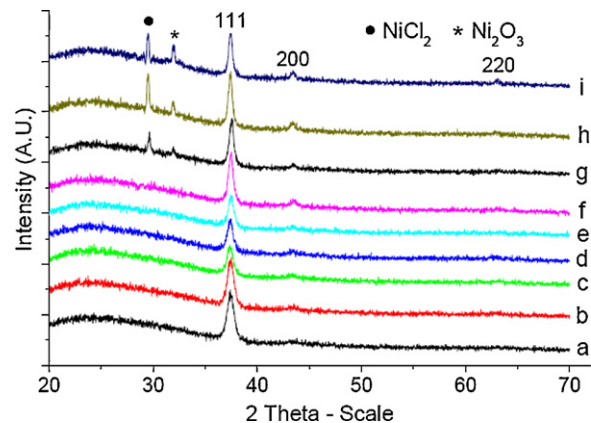


Fig. 2. X-ray diffraction patterns of various (Li:Ni) O_x alloy films: (a) undoped NiO, (b) NiO:Li (10 at%), (c) NiO:Li (20 at%), (d) NiO:Li (30 at%), (e) NiO:Li (40 at%), (f) NiO:Li (50 at%), (g) NiO:Li (60 at%), (h) NiO:Li (80 at%) and (i) NiO:Li (100 at%). Ni concentration is 0.1 M and $T_{\text{sub}} = 450^\circ\text{C}$.

Table 1
Summary of XRD parameters and mean grain size of all sample for (1 1 1) orientation.

Sample	2θ ($^{\circ}$)	Lattice distance (\AA)	FWHM ($^{\circ}$)	Mean grain size (nm)	Identification with (hkl) value
<i>(a) The effect of Ni concentration in solution ($T_{\text{sub}} = 450^{\circ}\text{C}$)</i>					
0.05 M	–	–	–	–	–
0.1 M	37.35	2.409	0.724	12.38	Cubic-NiO
0.15 M	37.38	2.417	0.551	16.23	Cubic-NiO
0.2 M	37.40	2.415	0.499	17.90	Cubic-NiO
<i>(b) The effect of substrate temperature (Ni concentration = 0.1 M)</i>					
350 $^{\circ}\text{C}$	37.41	2.402	1.112	8.03	Cubic-NiO
400 $^{\circ}\text{C}$	37.50	2.394	0.972	9.11	Cubic-NiO
450 $^{\circ}\text{C}$	37.48	2.397	0.696	12.76	Cubic-NiO
500 $^{\circ}\text{C}$	–	–	–	–	–
550 $^{\circ}\text{C}$	–	–	–	–	–
<i>(c) The effect of Li doping (Ni concentration = 0.1 M and $T_{\text{sub}} = 450^{\circ}\text{C}$)</i>					
Un-doped NiO	37.40	2.403	0.787	11.35	Cubic-NiO
NiO:Li (10 at%)	37.50	2.396	0.674	13.17	Cubic-NiO
NiO:Li (20 at%)	37.36	2.405	0.655	13.68	Cubic-NiO
NiO:Li (30 at%)	37.46	2.399	0.621	14.32	Cubic-NiO
NiO:Li (40 at%)	37.44	2.400	0.575	15.49	Cubic-NiO
NiO:Li (50 at%)	37.52	2.395	0.496	17.88	Cubic-NiO
NiO:Li (60 at%)	37.56	2.393	0.464	19.08	Cubic-NiO
NiO:Li (80 at%)	37.44	2.400	0.425	20.95	Cubic-NiO
NiO:Li (100 at%)	37.42	2.402	0.404	22.07	Cubic-NiO

The results of the electrical measurements for the undoped and alloy films have been summarized in Table 2. The thickness of the films was determined from transmission data using the Puma software [30]. As seen in this table, undoped NiO films deposited at the optimal condition exhibit the lowest sheet resistance. The electrical measurements for (Li:Ni) O_x alloy films show that the resistance of the films decreases with increasing Li-doping up to 50 at% and then increases. The lowest sheet resistance was obtained for doping level of 50 at%. The Hall effect experiment results

reveal that the majority carriers are holes for all samples (p-type conductivity).

3.2. Thermoelectrical properties

Fig. 4(a)–(c) shows the measured Seebeck coefficients versus temperature for undoped NiO and (Li:Ni) O_x alloy films. The positive sign of the Seebeck coefficients of the films confirms the p-type conductivity. As shown in Fig. 4(a), the highest value of the Seebeck

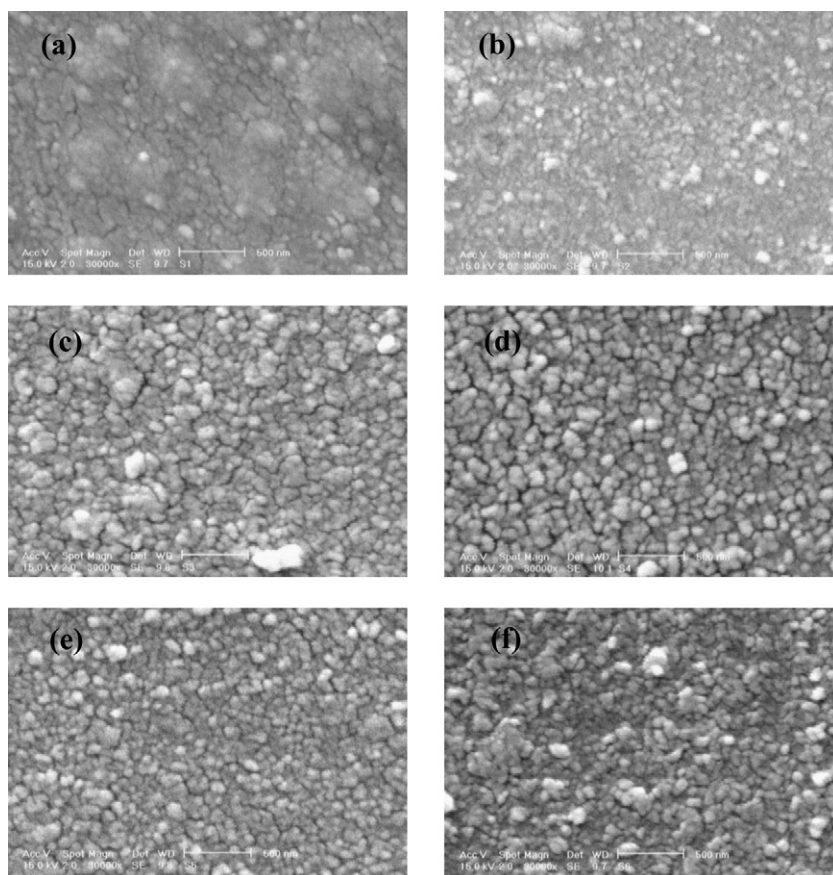


Fig. 3. SEM images of undoped and (Li:Ni) O_x alloy films: (a) Undoped NiO, (b) NiO:Li (20 at%), (c) NiO:Li (40 at%), (d) NiO:Li (50 at%), (e) NiO:Li (60 at%) and (f) NiO:Li (100 at%).

Table 2The electrical measurement results for the undoped and Li-doped NiO films. Thickness determination error is $\sim\pm 5\%$.

Sample	R_S ($M\Omega/\square$)	Carrier concentration (cm^{-3})	Thickness (t), (nm)
<i>(a) The effect of solution concentration ($T_{sub} = 450^\circ C$)</i>			
0.05 M	82.5	2.21×10^{15}	170
0.1 M	25.6	6.35×10^{15}	190
0.15 M	29.3	6.67×10^{15}	220
0.2 M	36.2	7.11×10^{15}	240
<i>(b) The effect of substrate temperature (Ni concentration = 0.1 M)</i>			
350 °C	34.3	2.37×10^{15}	260
400 °C	23.7	3.38×10^{15}	230
450 °C	20.6	6.93×10^{15}	195
500 °C	53.1	8.72×10^{14}	135
550 °C	71.8	7.96×10^{14}	95
<i>(c) The effect of Li doping ($T_{sub} = 450^\circ C$ and Ni concentration = 0.1 M)</i>			
Un-doped NiO	21.9	6.50×10^{15}	187
NiO:Li (10 at%)	18.9	2.16×10^{16}	190
NiO:Li (20 at%)	15.4	1.02×10^{17}	194
NiO:Li (30 at%)	13.6	1.14×10^{18}	197
NiO:Li (40 at%)	13.3	4.20×10^{17}	202
NiO:Li (50 at%)	4.7	1.91×10^{17}	205
NiO:Li (60 at%)	5.3	4.87×10^{15}	209
NiO:Li (80 at%)	7.7	4.15×10^{15}	214
NiO:Li (100)at%	16.6	3.58×10^{15}	219

coefficients belongs to the undoped sample prepared with 0.1 M Ni concentration in the precursor solution. Fig. 4(b) shows that the undoped sample deposited at 450 °C has the largest Seebeck coefficient among the ones prepared with other substrate temperatures. In case of the Li-doped films, Fig. 4(c) shows that for the sample with 50 at% doping level, the value of Seebeck coefficient is the highest among the samples with other doping levels.

The variation of thermoelectric e.m.f. versus temperature difference between the two ends of samples (δT) is shown in Fig. 5(a)–(c). Fig. 5(a) and (b) belongs to the undoped NiO samples. Fig. 5(c) shows that the highest thermoelectric e.m.f. is ~ 80 mV ($\delta T = 160$ K) corresponding to the 50 at% Li-doped sample.

3.3. Optical properties

Optical transmittance of the undoped NiO and (Li:Ni) O_x films in 300–1100 nm range is shown in Fig. 6(a)–(c). In case of undoped films deposited with different Ni concentration (Fig. 6(a)), the average transmittance decreases from $\sim 90\%$ to $\sim 70\%$ when the Ni molarity changes from 0.05 M to 0.2 M ($T_{sub} = 450^\circ C$) due to increase in the film thickness [28]. In contrast, Fig. 6(b) shows that the optical transparency of undoped films increases from $\sim 60\%$ to $\sim 95\%$ when the substrate temperature increases from 350 °C to 550 °C (Ni concentration = 0.1 M). Transparency of the Li-doped NiO films decreases from $\sim 80\%$ to $\sim 50\%$ when the doping level increases from 0 at% to 100 at% under optimal deposition condition (Fig. 6(c)). This can be also attributed to the increase in the film thickness [14].

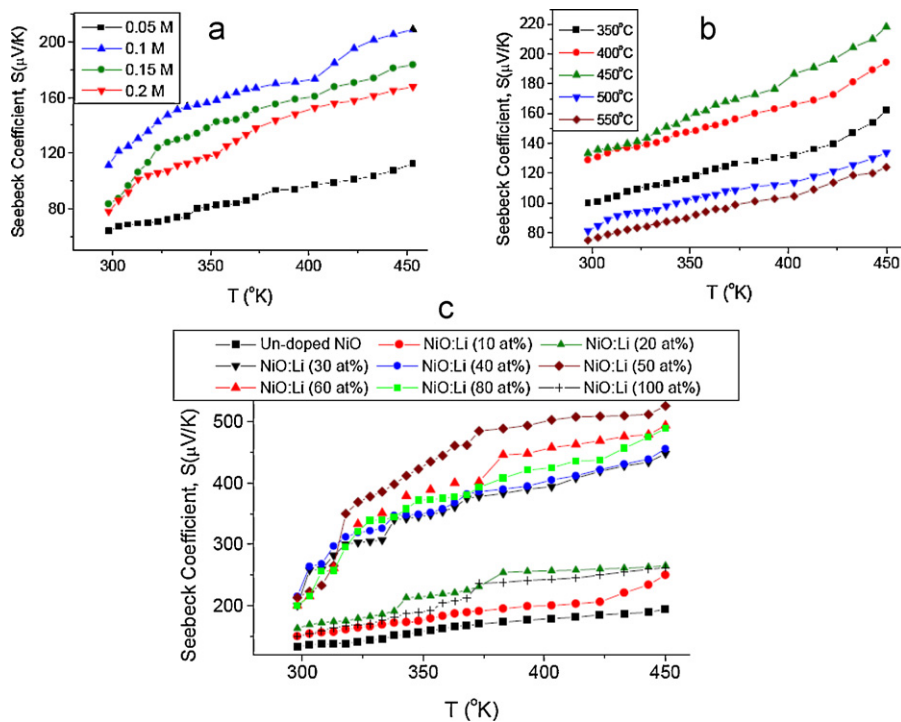


Fig. 4. Seebeck coefficient (S) versus temperature for: (a) Undoped samples with different Ni concentration in the solution ($T_{sub} = 450^\circ C$), (b) undoped samples deposited on substrates with different temperatures (Ni concentration = 0.1 M), and (c) Li-doped NiO films with different doping levels.

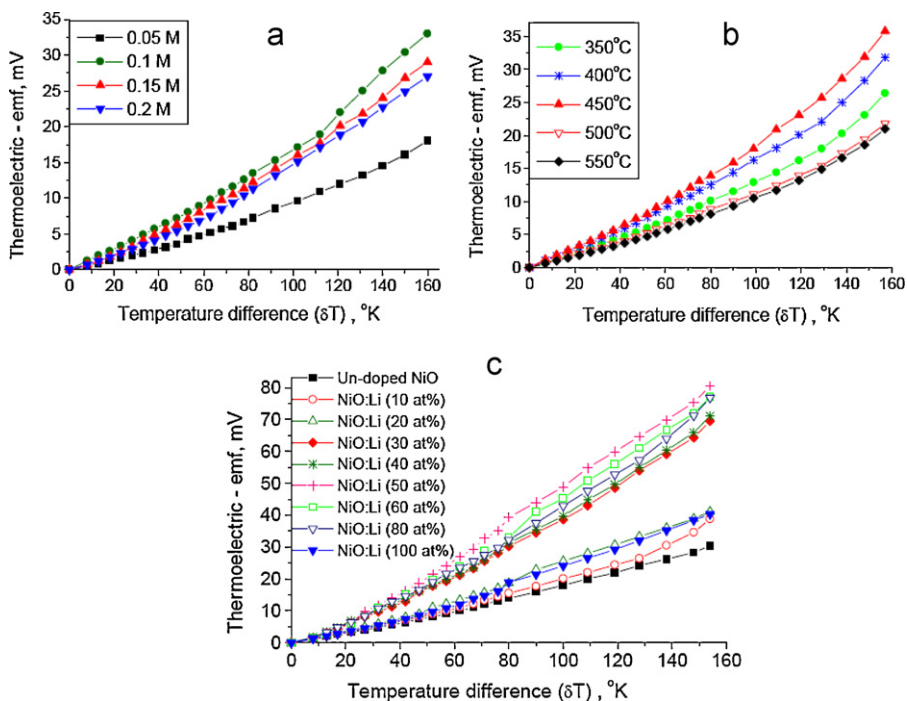


Fig. 5. The variation of thermoelectric e.m.f. with temperature difference (ΔT) for: (a) undoped samples with different Ni concentration in the solution ($T_{\text{sub}} = 450^\circ\text{C}$), (b) undoped samples deposited on substrates with different temperatures (Ni concentration = 0.1 M), and (c) Li-doped NiO films deposited with different level of doping.

Fig. 7(a)–(c) presents the variation of $(\alpha h\nu)^2$ versus $h\nu$ (photon energy) for the films, in which α is the absorption coefficient. The optical band gap has been calculated by extrapolation of linear part of the curve. As seen in Fig. 7(a), the optical band gap gradually decreases from 3.718 eV to 3.515 eV by increasing Ni concentration in the solution from 0.05 M to 0.2 M when $T_{\text{sub}} = 450^\circ\text{C}$. This may be attributed to the increase in the film thickness as well as the crystalline order and increasing grain size [28]. Fig. 7(b) shows that the band gap of the undoped NiO

films decreases from 3.704 eV to 3.627 eV when the substrate temperature increases from 350°C to 450°C (due to grain size increase [29]) and then increases for temperatures up to 550°C . This increase could be related to the amorphous structure of films deposited at high substrate temperature. In amorphous materials, electron transitions may be either from localized states in the conduction band or from extended states in the valence band to localized states at the conduction edge. This leads to lower energies than those for polycrystalline or bulk crystalline materials

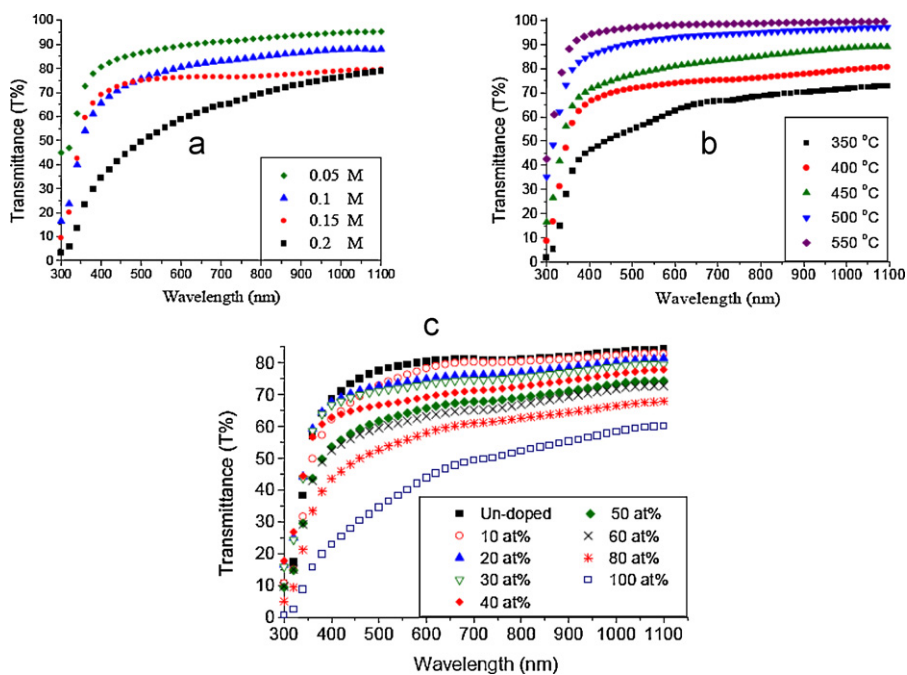


Fig. 6. Optical transparency of: (a) undoped samples with different Ni concentration in the solution ($T_{\text{sub}} = 450^\circ\text{C}$), (b) undoped samples deposited on substrates with different temperatures (Ni concentration = 0.1 M), and (c) Li-doped films deposited with different Li concentration.

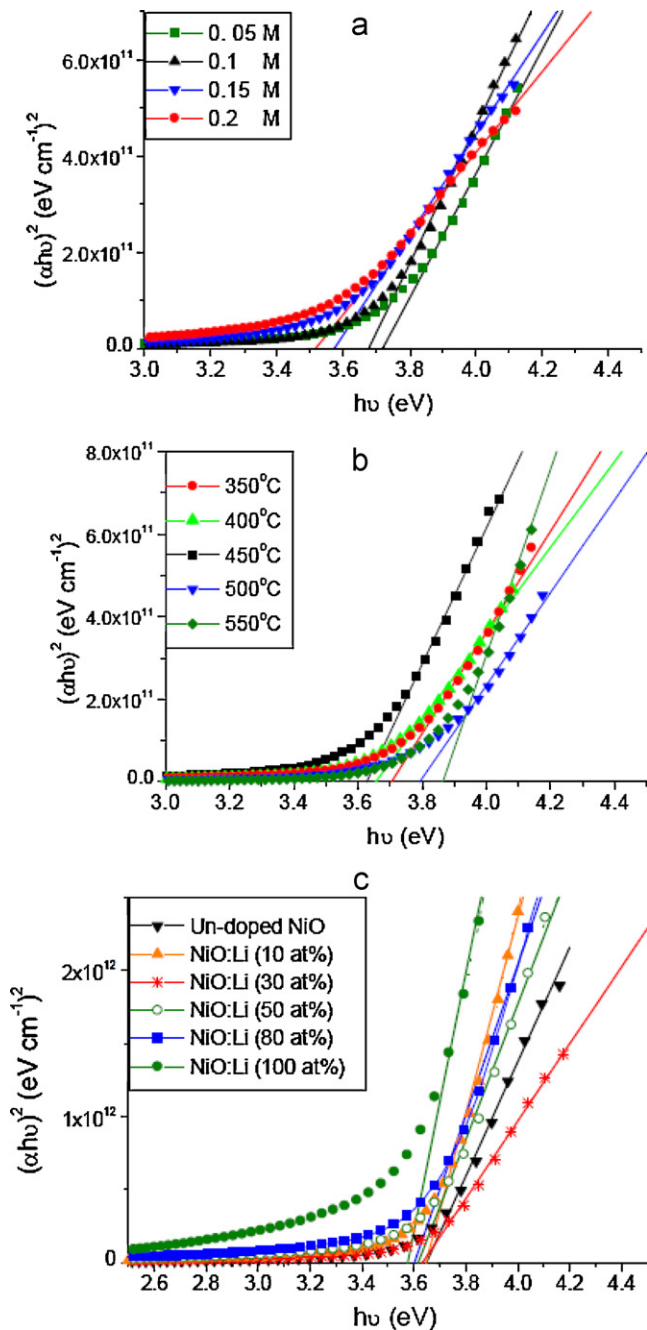


Fig. 7. Plots of $(\alpha hv)^2$ versus $h\nu$ (photon energy) for: (a) undoped NiO films prepared with different Ni concentration in solution ($T_{\text{sub}} = 450^\circ\text{C}$), (b) undoped samples deposited at different substrate temperature (Ni concentration = 0.1 M), and (c) Li-doped NiO films with different doping levels.

[31,32]. The optical band gap of $(\text{Li:Ni})\text{O}_x$ alloy films decrease from 3.647 eV to 3.580 eV, which is related to the grain size increase (Fig. 7(c)).

4. Conclusions

In this paper, we report the preparation and characterization of undoped NiO and $(\text{Li:Ni})\text{O}_x$ alloy thin films. These films have been deposited on glass substrates by spray pyrolysis technique. Physical properties of prepared undoped films with different nickel concentrations in precursor solution, different substrate temperatures,

and various Li-doping levels have been investigated. It is observed that the physical properties of films strongly depend on the deposition conditions and Li-doping levels. The obtained results lead to the following conclusions:

- (1) The prepared films exhibit a preferential growth along the (1 1 1) direction with a cubic NiO phase. With increasing the Ni concentration in precursor solution and substrate temperature, the (1 1 1) peak intensity is enhanced and crystallite size increases. Also, at 60 at%, 80 at% and 100 at% Li doping levels, other phases such as Ni_2O_3 and NiCl_2 are observed.
- (2) Electrical measurements of the samples show that the sheet resistance of the films decreases with increasing Ni concentration up to 0.1 M and substrate temperature up to 450°C . Also, the lowest resistance was obtained to be $4.7 (\text{M}\Omega/\square)$ for doping level of 50 at%. The Hall effect and thermoelectrical measurements have shown p-type conductivity in all films. The highest Seebeck coefficient was $503 \mu\text{V/K}$ at 400 K for 50 at% Li-doping.
- (3) The transparency of the films decreases with increasing Ni concentration and increases with increasing the substrate temperature. In case of $(\text{Li:Ni})\text{O}_x$ alloy films, transparency decreases from $\sim 80\%$ to $\sim 50\%$ when the doping level increases from 0 at% to 100 at%.

References

- [1] Z.Q. Li, J.J. Lin, J. Appl. Phys. 96 (2004) 5918–5920.
- [2] C.G. Granqvist, A. Hultaker, Thin Solid Films 411 (2002) 1.
- [3] H. Hosono, Thin Solid Films 515 (2007) 6000–6014.
- [4] Y. Hoshi, T. Kiyomura, Thin Solid Films 411 (2002) 36–41.
- [5] J. Zhao, L. Hu, W. Liu, Z. Wang, Appl. Surf. Sci. 253 (2007) 6255–6258.
- [6] C. Körber, P. Agoston, A. Klein, Sens. Actuators B 139 (2009) 665–672.
- [7] M. Kitao, K. Izawa, K. Urabe, T. Komatsu, S. Kuwano, S. Yamada, Jpn. J. Appl. Phys. 33 (1994) 6656.
- [8] I.M. Chan, F.C. Hong, Thin Solid Films 450 (2004) 304.
- [9] H. Kumagai, M. Matsumoto, K. Toyoda, M. Obava, J. Mater. Sci. Lett. 15 (1996) 1081.
- [10] J. Bandara, C.M. Divarathne, S.D. Nanayakkara, Sol. Energy Mater. Sol. Cells 81 (2004) 429.
- [11] R.K. Gupta, K. Ghosh, P.K. Kahol, Physica E 41 (2009) 617–620.
- [12] G. Boschloo, A. Hagfeldt, J. Phys. Chem. B 105 (2001) 3039.
- [13] J.D. Desai, S.K. Min, K.D. Jung, O.S. Joo, Appl. Surf. Sci. 253 (2006) 1781–1786.
- [14] D.P. Joseph, M. Saravanan, B. Muthuraaman, P. Renugambal, S. Sambasivam, S.P. Raja, P. Maruthamuthu, C. Venkateswaran, Nanotechnology 19 (2008) 485707.
- [15] U.S. Joshi, Y. Matsumoto, K. Itaka, M. Sumia, H. Koinuma, Appl. Surf. Sci. 252 (2006) 2524–2528.
- [16] Y. Nakamura, H. Ogawa, T. Nakashima, A. Kishimoto, H. Yanagida, J. Am. Ceram. Soc. 80 (1997) 1609.
- [17] H. Ohta, M. Kamiya, T. Kamiya, M. Hirano, H. Hosono, Thin Solid Films 445 (2003) 317.
- [18] J.W. Lee, I.H. Park, C.W. Chung, Integr. Ferroelectr. 74 (2005) 71.
- [19] H.L. Chena, Y.M. Lub, W.S. Hwang, Surf. Coat. Technol. 198 (2005) 138–142.
- [20] D. Franta, B. Negulescu, L. Thomas, P.R. Dahoo, M. Guyot, I. Ohlídal, J. Mistrík, T. Yamaguchi, Appl. Surf. Sci. 244 (2005) 426–430.
- [21] H. Sato, T. Minami, S. Tanaka, T. Yamada, Thin Solid Films 236 (1993) 27.
- [22] K. Nishita, A. Koma, K. Saiki, J. Vac. Sci. Technol. A 19 (2001) 2282.
- [23] R.C. Korosec, P. Bukovec, Acta. Chim. Slov. 53 (2006) 136–147.
- [24] P.S. Patil, L.D. Kadam, Appl. Surf. Sci. 199 (2002) 211–221.
- [25] L. Cattin, B.A. Reguig, A. Khelil, M. Morsli, K. Benchouk, J.C. Bernede, Appl. Surf. Sci. 254 (2008) 5814–5821.
- [26] M.-M. Bagheri-Mohagheghi, N. Shahtahmasebi, M.R. Alinejad, A. Youssefi, M. Shokooh-Saremi, Solid State Sci. 11 (2009) 233–239.
- [27] M.-M. Bagheri-Mohagheghi, N. Shahtahmasebi, M.R. Alinejad, A. Youssefi, M. Shokooh-Saremi, Physica B 403 (2008) 2431–2437.
- [28] S.A. Mahmud, A.A. Akl, H. Kamal, K. Abdel-Hady, Physica B 311 (2002) 366–375.
- [29] H. Kamal, E.K. Elmaghraby, S.A. Ali, K. Abdel-Hady, J. Cryst. Growth 262 (2004) 424–434.
- [30] E.G. Birgin, I. Chambouleyron, J.M. Martínez, J. Comput. Phys. 151 (1999) 862–880.
- [31] A.F. Aktaruzzaman, G.L. Sharma, L.L. Malhotra, Thin Solid Films 198 (1991) 67–74.
- [32] P. Puspharajah, S. Radhakrishna, A.K. Arof, J. Mater. Sci. 32 (1997) 3001–3006.